Available online at www.sciencedirect.com
ScienceDirect
Solar Energy Materials & Solar Cells 92 (2008) 651–659
Solar Energy Materials and Solar Cells
www.elsevier.com/locate/solmat

Towards optimization of device performance in conjugated polymer photovoltaics: Charge generation, transfer and transport in poly(*p*-phenylene-vinylene) polymer heterojunctions

Stephanie V. Chasteen[a,*], Veronica Sholin[b], Sue A. Carter[b], Garry Rumbles[c]

[a]*Physics Department, University of Colorado-Boulder, 390 UCB, Boulder, CO 80309-0390, USA*
[b]*Physics Department, University of California-Santa Cruz, ISB, Santa Cruz, CA 95064, USA*
[c]*Center for Basic Science, MS 3216, 1617 Cole Blvd., National Renewable Energy Laboratory, Golden, CO 80401, USA*

Received 19 October 2007; received in revised form 25 January 2008; accepted 25 January 2008

Abstract

We fabricate photovoltaics comprised layers and blends of a hole-transporting derivative of poly(*p*-phenylene-vinylene) with a variety of electron-transporters: titanium dioxide, a cyano-substituted PPV, and a fullerene derivative (PCBM) to enhance device performance. Photovoltaic device characterization is combined with time-resolved and steady-state photoluminescence to understand the nature of the excited state and its effect upon device performance. We find that morphological differences, such as chain conformation or domain size, often overshadow the effect of charge transfer, so that device performance is not necessarily correlated with rapid decay times. Exciton generation is found to be a similarly important factor in most devices. These results provide insight into non-optimized device morphologies.

Keywords: Organic photovoltaic; Photoluminescence; Time-resolved; Heterojunction; Fullerene

1. Introduction

Despite record high efficiencies, the photovoltaic market is hindered by the high price of photovoltaic production. One promising candidate in the quest to reduce material cost is organic photovoltaics [1–5], which have been the subject of much research. Organics offer the potential for low-temperature, large area processing (e.g., screen-printing and ink-jet printing), allowing them to be printed on flexible substrates at reduced cost.

In order for organic photovoltaics to break into the marketplace; however, they must overcome the twin hurdles of low efficiencies and short lifetimes. Because of the instability of the vinylene bond in PPV materials, performance degradation in response to exposure to air and light is a serious issue [6–9], which is being addressed in other research efforts [10–12].

Most estimates suggest that device efficiency must reach 5–10% in the laboratory before commercialization is possible. Recent works on blended films optimized for film morphology have approached this benchmark [13,14]. The improvement of organic device architecture has been hampered in part by an incomplete understanding of many of the fundamental physical processes involved in the operation of these cells, as well as the need to optimize materials and morphology for charge generation and transport, as addressed in several recent reviews [15–17].

The performance of organic photovoltaics is severely limited by poor exciton dissociation and charge transport due in part to high rates of exciton recombination and low charge mobilities in polymers. This challenge can be partially met through the use of blended and layered heterojunctions. Such morphologies offer multiple exciton dissociation sites and separate charge pathways, thus limiting exciton recombination, and allowing for thicker, more absorbing, polymer films. Since the exciton must be formed within the exciton diffusion length (~10 nm) of an

*Corresponding author. Tel.: +1 303 775 3277.
E-mail address: Stephanie.chasteen@colorado.edu (S.V. Chasteen).

0927-0248/$ - see front matter © 2008 Elsevier B.V. All rights reserved.
doi:10.1016/j.solmat.2008.01.014

interface in order to be dissociated, any material further away from the interface does not contribute to the photocurrent, limiting the thickness of layered devices. The primary advantage of nanoscale blended (bulk heterojunction) devices over planar layers is their ability to harvest more useful light through the use of thicker, more absorbing films.

A challenge in blended devices is controlling phase separation on a nanometer scale. The use of highly volatile solvents, which evaporate quickly, help keep the domain size small because energetic equilibrium is not reached in these immiscible blends. One main drawback to blended structures is that charge transport is often compromised. In blends, charges must hop from domain to domain, and there is often not a clear path from one electrode to the other, unlike layered structures.

It can be difficult to discern the underlying charge generation, transport, and transfer processes in polymer-based optoelectronic devices. Spectroscopic analysis allows insight into the various competing mechanisms that deactivate the excited state, such as intersystem crossing, internal conversion, fluorescence, and quenching via charge- or energy-transfer. The observed molecular lifetime (excluding bimolecular processes) is given by the reciprocal of the sum of all rate constants: $\tau = 1/k_r + k_{nr} + k_D[Q]$, where k_r is the rate of radiative decay, k_{nr} of non-radiative decay, and k_D of dissociation via transfer to an external quencher with concentration Q. Along with steady-state photoluminescence spectroscopy, time-resolved photoluminescence spectroscopy can be a powerful tool for probing the excited state dynamics, exciton dissociation, and charge transfer process. In addition, device properties, such as current–voltage characteristics, combined with morphology measurements and numerical simulations can yield insight into the charge generation and transport process. In this paper, we have fabricated photovoltaic devices combining hole-transporting polymers with a variety of electron-transporters and have utilized steady-state and time-resolved spectroscopy combined with device characterization, morphological studies, and numerical simulations, to understand the role that charge generation, exciton dissociation, and charge transport have on optimizing the device performance in polymer PVs.

2. Materials

Material structures are shown in Fig. 1 and their respective estimated energy levels at zero bias are shown in Fig. 2. Our hole-transporting polymer, M3EH-PPV, is a strictly alternating copolymer of the well-characterized semiconducting polymer poly(2-methoxy-5-(2′-ethylhexyloxy)-1,4-phenylene-vinylene) or MEH-PPV. MEH-PPV is a derivative of poly-phenylene-vinylene (PPV) asymmetrically substituted with alkoxy groups, which confer solubility and create a narrow band gap. M3EH-PPV was synthesized by Horner reaction and has optical properties very similar to MEH-PPV [18]; however, due

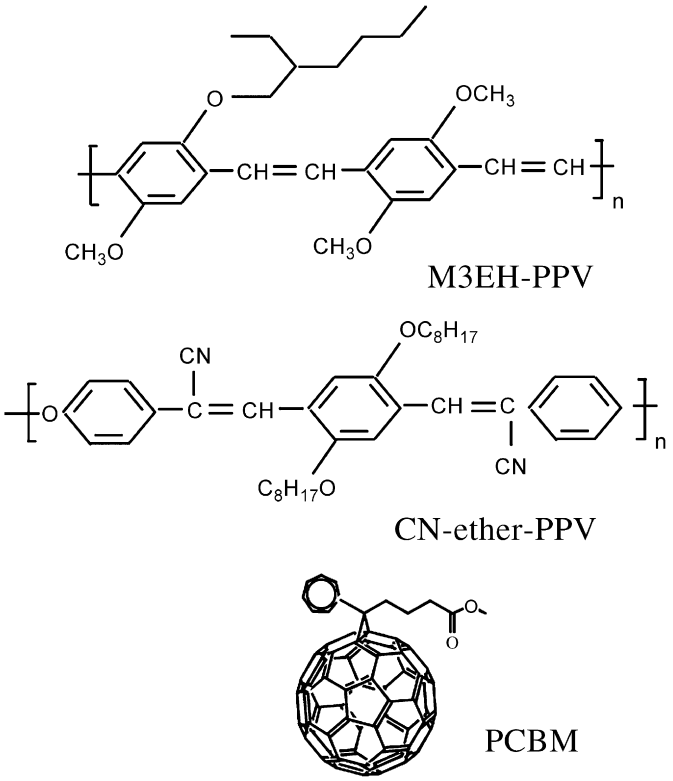

Fig. 1. Structures of materials used.

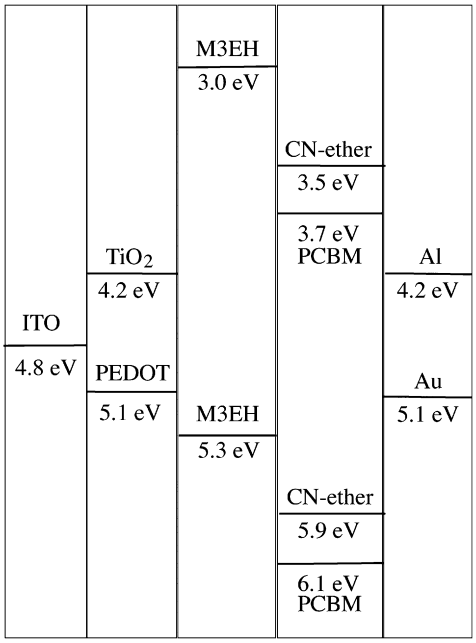

Fig. 2. Conduction and valence bands of materials used.

to the limited length of the side-chains, M3EH-PPV is much less soluble than MEH-PPV and enables multi-layered structures as well as a greater hole mobility. Compared to MEH-PPV, M3EH-PPV has been found to have twice the zero-field mobility [19] ($5 \times 10^{-7}\,cm^2/V\,s$) about twice the glass transition temperature (113 °C), and a higher number average molecular weight (44,300) as

determined by gel permeation chromatography (GPC) [19]. The high glass transition temperature indicates a more ordered structure requiring greater energy input in order to initiate a phase transition from an ordered to glassy phase. Its photoluminescence quantum efficiency is similar to that of MEH-PPV [20]. M3EH-PPV has HOMO and LUMO levels of 5.3 and 3.0 eV, respectively. The exciton diffusion length is expected to be around 10 nm, similar to other PPV materials [21].

As electron-transporters we used a metal oxide, a PPV-based polymer and a fullerene derivative. Our metal oxide is the TiO_x layer present in some architectures, as described below. Poly[oxa-1,4-phenylene-1,2-(1-cyano)-ethenylene-2,5-dioctyloxy-1,4-phenylene-1,2-(2-cyano)-ethenylene-1,4-phenylene] or CN-ether-PPV (Fig. 1) is a derivative of poly(2,5,2′,5′-tetrahexyloxy-8,7′-dicyano-di-*p*-phenylenevinylene), or CN-PPV, and is designed to increase solubility and electron affinity relative to CN-PPV. CN-ether-PPV was obtained courtesy to the University of Jena in Germany and synthesized as described elsewhere [22]. It is nearly identical in structure to the conjugated polymer PCNEPV, used by another group [23,24]. It has HOMO and LUMO levels of 5.9 and 3.5 eV, respectively. Phenyl-C61-butyric acid methyl ester (PCBM) [25] is a derivative of buckminsterfullerene, with a HOMO and LUMO of 6.1 and 3.7 eV, respectively.

Charge transfer from polymers to PCBM is known to be rapid and efficient. The addition of just a few percent by weight of PCBM results in luminescence quenching of three orders of magnitude, because charge transfer to PCBM occurs within ~50 fs—three orders of magnitude faster than the radiative recombination which competes even with the vibronic relaxation of the excitations [26,27]. The high electron mobility of PCBM (at least three orders of magnitude higher than those in PPV) is advantageous to device performance, but the mismatch in carrier mobility leads to space-charge limited current [28]. The percolation threshold of PCBM is 17 vol% [29], corresponding to about 25 wt%, with best performance around 60–80 wt% due to a compromise between absorption, charge separation, and material mobilities [30]. Past 60 wt% the combination of charge separation and mobility reaches an optimum value [31] due to the formation of large PCBM domains which enable the transport of electrons across the device. Surprisingly, the hole-transport properties in the polymer can also be enhanced by the addition of PCBM, by up to two orders of magnitude [30,32–34], perhaps due to the enhancement of interchain interactions. The closer match between electron and hole mobilities results in enhanced device performance due to reduced charge buildup [13,30].

3. Methods

Our photovoltaics are built in a sandwich structure on indium tin oxide (ITO) coated glass. Either PEDOT-PSS or titanium dioxide (TiO_2) is used for the transparent material deposited on top of the ITO substrate, resulting in opposite polarity devices due to differential work function steps (see Fig. 2). A transparent semiconductor, TiO_2, acts as an electron-transporter and hole-blocker due to its extremely low-lying HOMO. When light is incident on TiO_2, it becomes relatively conducting so that the quasi-Fermi-level of the photodoped TiO_2 appears to play an important role in determining the open circuit voltage. PEDOT-PSS (Bayer) is polyethelynedioxythiophene with polystyrene-sulfonate. It has a substantially larger work function (~5.1 eV) than ITO (~4.8 eV), and thus acts as a hole-acceptor as well as a planarizing layer. PEDOT-PSS is deposited by spin-casting at 3000 rpm, and then heating to 120 °C under vacuum to remove water from the film. Titanium dioxide is deposited as a smooth TiO_x sol–gel [35], spin-cast at ~1000 rpm to produce a uniform film 50–100 nm thick, then sintered at 450 °C for 30–60 min to convert the material to a crystalline anatase phase. The TiO_x film is transparent and smooth, with surface features less than 3 nm. Both TiO_2 and PEDOT-PSS have been shown to improve device performance over bare ITO [36,37].

Polymers are dissolved by weight fraction (~0.7–1.3%) in chlorobenzene or toluene and allowed to form uniform solutions by leaving on a heated stirplate for 2–24 h. Once dissolved, polymers are spin-cast by pipetting a small amount (approximately 50 μL) onto the PEDOT or TiO_2-coated substrate, and spinning at 1000–4000 rpm. This creates films from 15 to 200 nm thick, depending upon spin-speed and solution concentration. Upon spin-casting, polymer films are annealed at a temperature of 100 °C for 1 h. When the polymer films are heated past the glass-transition temperature, the polymer chains untangle to form a lower energy configuration, which leads to a semicrystalline structure and, presumably, better chain packing [38]. Device performance is enhanced upon annealing [39] and the photoluminescence red-shifts and is reduced in intensity, indicating the formation of interchain contacts characteristic of more crystalline films [38]. The top electrode (generally Al or Au) is then deposited under vacuum by thermal evaporation.

Thickness measurements are made using an atomic force microscope in contact mode. Current density vs. voltage curves was measured using a 2400 Keithley source meter. Illumination is typically provided by a white light bulb with an output of approximately 160 mW/cm^2. Because this light source is a poor match with AM1.5, both in terms of intensity and spectral output, short-circuit current densities are given for relative purposes only.

Absorption spectra are taken on a Varian optical spectrometer. Steady-state photoluminescence spectra were recorded using a Fluorolog-3 (JYHoriba) spectrometer that utilized a liquid N_2 cooled CCD detector to minimize thermal noise. Monochromatic excitation light was generated by a Xenon arc lamp with double monochromator. Fluorescence was collected at 22° for film (90° for solutions) relative to the excitation beam, passed through a

single monochromator containing a 300 line/mm grating and imaged on the liquid nitrogen-cooled CCD array. The emission spectra are corrected for the wavelength response of the spectrograph and CCD detector, and their intensity normalized against the intensity of the excitation light.

Fluorescence decay signals were measured using the technique of time correlated single photon counting (TCSPC) [40]. The excitation source was a pulsed, picosecond diode laser (IBH NanoLED-10) with a pulse width of 110 ps, operating at a wavelength of 438 nm and a repetition rate of 1 MHz. Emission was detected at 90° and 22° to excitation for solution and film, respectively, by focusing the emission onto the slits of a 0.25 m monochromator (SPEX minimate), and subsequently detected by a photon counting photomultiplier tube (Hamamatsu H6279). The PMT output was amplified using a 1 GHz amplifier (Philips model 6954) then shaped using a constant fraction discriminator (Ortec, Tennelec model 583). The resulting signal was fed into the start input of a time-to-amplitude converter, (TAC, Ortec, model TC864), which was operated in reverse mode. The stop input to the TAC was supplied by an output directly from the pulsed laser diode controller (IBH NanoLED-C). The TAC output was fed to a multi-channel analyzer (Oxford Instruments PCA3-8 K) operating in pulse-height analysis mode. A variety of parameters are used to judge whether a fitted function is a good approximation of the data [40], including reduced chi square, Durbin–Watson parameter, and plot of the weighted residuals.

4. Results

4.1. Pristine M3EH-PPV

The performance of M3EH-PPV heterojunction devices is compared in Fig. 3. Pure M3EH-PPV devices are dominated by hole-transport. Devices on the TiO_2//Au structure (transparent cathode structure; $J_{sc} = 0.9\,mA/cm^2$, $V_{oc} = 0.75\,V$, FF = 42%)) outperform those on the PEDOT//Al structure (transparent anode; $J_{sc} = 0.07\,mA/cm^2$, $V_{oc} = 0.96\,V$, FF = 22%) by an order of magnitude. The reversed polarity in PEDOT//Al forces

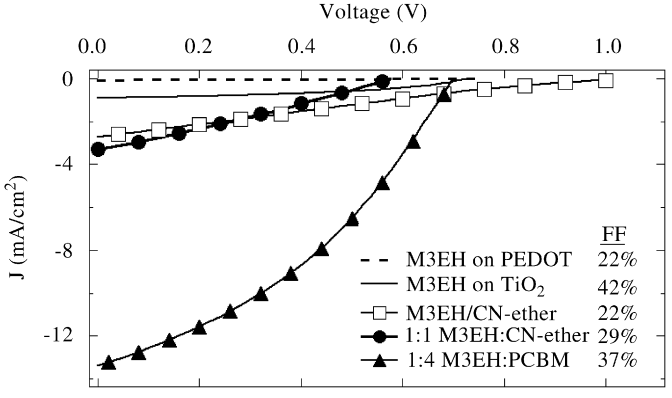

Fig. 3. *J–V* curves for M3EH-PPV heterojunction devices.

the poorly mobile electrons to cross the bulk of the device from the PEDOT/polymer interface. This process is extremely inefficient, and so the bulk of the photocurrent arises from dissociation at the polymer/Al interface; hence, the observation of an antibatic spectral response (data not shown). Only a small portion of the incident light is able to reach this interface, resulting in low photocurrents and fill-factors. Time-resolved photoluminescence decays for neat M3EH-PPV films are shown graphically in Fig. 5, and the associated decay times are reported in Table 1. All heterojunctions are quenched relative to the pristine polymers (though only for the shortest decay time, $\tau_1 = 0.20 \pm 0.04$ ns).

4.2. Titanium dioxide

The improvement in device performance for TiO_2//Au structures (as compared to PEDOT//Al) is found to be primarily due to the electric field reversal in these devices, as opposed to exciton dissociation, since TiO_2 is found to be an inefficient electron acceptor. No quenching is observed in the steady-state or time-resolved photoluminescence for M3EH-PPV deposited on smooth TiO_x sol–gel, rough TiO_2 nanoparticles, or nanoporous TiO_2 slurry, despite attempts to reduce the signal from the bulk by deposition of thin (~10 nm) polymer films, as explored in a recent study [41]. We note that these results contrast with those observed by Scully and McGehee for MDMO-PPV on titania, in which the fluorescence of a 15 nm film was quenched by more than 90% [28].

In comparison, fluorescence quenching was observed in bi-layered M3EH-PPV/CN-ether-PPV devices, even at relatively high film thicknesses (~50 nm), indicating that TiO_2 is simply a less efficient quencher than CN-ether-PPV.

4.3. CN-ether-PPV

Combining M3EH-PPV with the electron-transporter CN-ether-PPV resulted in improvements in device performance due to increased charge separation and reduced loss to recombination. Results on M3EH-PPV:CN-ether-PPV blends and layers and the associated decay times are reported in more detail elsewhere [42]. A balance in the mobilities of electrons and holes is important in order to reach high currents as this results in bipolar transport and avoids space-charge limited current. This was not achieved for blends of P3HT (poly-(3-hexylthiophene)) with CN-ether-PPV devices, presumably due to the higher hole mobility of P3HT compared to electron mobility of CN-ether-PPV, whereas the mobilities of M3EH-PPV and CN-ether-PPV appear to be better matched.

CN-ether-PPV is characterized by a long 14 ns decay component and a broad red-shifted emission, indicative of an emissive excimer state [43,44]. These excimers are particularly vulnerable to quenching via charge-transfer to other materials, and residual CN-ether-PPV decay components contribute to the overall decay in disproportionately

Table 1
Decay components for polymers in this study

	Film	η/η_{max}	τ_1 (ns) (% yield)	τ_2 (ns) (% yield)	τ_3 (ns) (% yield)	τ_{ave} (ns)	Q1 (%)	Q2 (%)
Pristine polymers	M3EH-PPV		0.20±0.04 (43%)	**0.45±0.09** (53%)		0.38		
	CN-ether-PPV	N/A	4.3±0.12 (26%)	**12.2±0.09** (**73%**)		10.0		
TiO_x layer	TiO_x/M3EH-PPV	0.1	0.12±0.03 (42%)	**0.32±0.10** (**44%**)		0.35	0	
CN-ether blends	50 wt% CN-ether	0.2	**0.05** (**51%**)	0.46 (20%)	2.0 (22%)	1.0	75	90
	M3EH/CN-ether layer	0.2	**0.05** (**39%**)	0.46 (17%)	2.0 (27%)	1.8	75	82
PCBM blends	80 wt% PCBM	1	0.05±0.01 (36%)	**0.50±0.04** (**49%**)	1.9±0.26 (16%)	0.6	75	
	50 wt% PCBM	**0.7**	0.02±0.01 (**73%**)	0.36±0.15 (14%)	1.3±0.05 (13%)	0.24	90	
	20 wt% PCBM	0.3	0.02±0.001 (**95%**)		1.0±0.022 (5%)	0.07	90	

Emission is at 600 nm and films are ~100 nm thick. Percent yield is the pre-exponential factor weighted by the decay time, and is reported in parentheses below each time component. The dominant decay component is highlighted in bold. All decays are fit to three exponentials; those with less than 10% yield are not reported for clarity. Q1 is the % quenching of the primary decay component of the hole-transporter M3EH-PPV (0.20 ns); Q2 is the % quenching of the average decay time of the electron-transporter CN-ether-PPV. Relative power conversion efficiency (η/η_{max}) is based upon the maximum power efficiency η_{max} measured for 80 wt% PCBM/polymer blends.

small amounts, suggesting that the long-lived excimer state is easily quenched even for small volume fractions of M3EH-PPV. CN-ether-PPV, therefore, serves as an efficient source of separable charge with a long radiative lifetime; these findings are important for design of materials for use in optoelectronic applications. Detailed results on CN-ether-PPV are reported in more detail elsewhere [45].

Blended and layered structures were characterized by similar optimized short-circuit currents and efficiencies, although blended devices tended to outperform layered structures. For blended structures, significant exciton quenching occurs in both the electron- and hole-transporting polymers due to the interpenetrating morphology (see Table 1); however, the lack of complete quenching limits the achievable short-circuit currents. In layered structures, decay times were longer than for blends (Fig. 5); thus exciton dissociation and charge transfer are more efficient in blended than in layered devices.

Given the poor dissociation efficiency in layers, we performed numerical simulations in order to determine the source of the high short-circuit currents in layered structures [42,46]. Simulations indicated that increased exciton generation (rather than charge separation) is the primary means of improved current in layered structures, due to reflected light from the Al electrode incident upon the polymer/polymer interface. Thus, the second polymer layer thickness must be carefully chosen in order to create an electric field maximum at the polymer/polymer interface: This places restrictions on further optimization of this device structure. These simulations also reveal that performance of M3EH-PPV/CN-ether-PPV layers is still limited by space-charge buildup due to a poor match between electron and hole mobilities.

Both steady-state and time-resolved PL data indicate that charge transfer occurs to an intermediate exciplex state in blended and layered structures of CN-ether-PPV with M3EH-PPV, as indicated in a previous publication [42]. The exciplex is characterized by a decay component of ~2.0 ns, which dominates at 700 nm emission, which corresponds to the spectral location of a broad, featureless peak in the steady-state attributed to exciplex emission. Formation of the exciplex aids device performance, as indicated by the dominance of the exciplex peak (and notable absence of M3EH-PPV emission) in steady-state spectroscopy on particularly efficient photovoltaic devices [47]. The exciplex may thermally re-excite the M3EH-PPV exciton, providing an additional route for charge separation, or dissociate directly under the influence of an electric field [48]. In either case, exciplex formation results in efficient charge generation, accounting for the high performance of 1:1 blended devices in which both polymers are present in sufficient volume fraction for charge transfer to the exciplex.

All blended and layered structures are characterized by poor fill factors (FFs), indicating poor charge-transport. The FF decreases as CN-ether-PPV is added to the blend (Fig. 4), indicating that exciton dissociation and charge-transport work at cross-purposes in these structures. Both blended and layered devices exhibit incomplete quenching of the excited state (Table 1) suggesting that the use of a better electron acceptor would enhance device performance, as observed for PCBM blends.

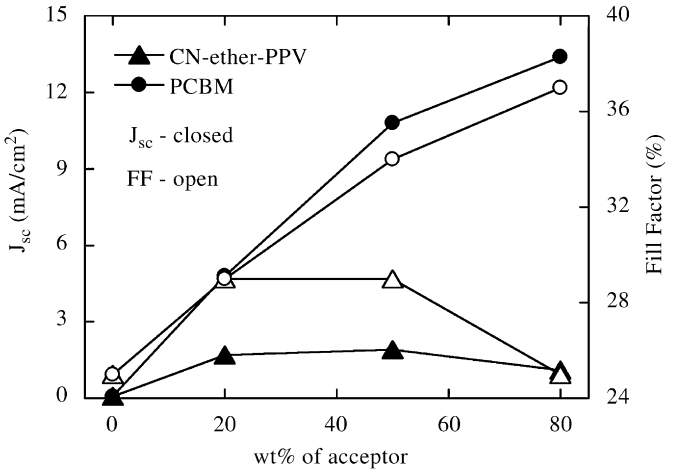

Fig. 4. Current (closed symbols) and fill factor (open symbols) versus wt% of CN-ether-PPV (triangles) and wt% of PCBM (circles).

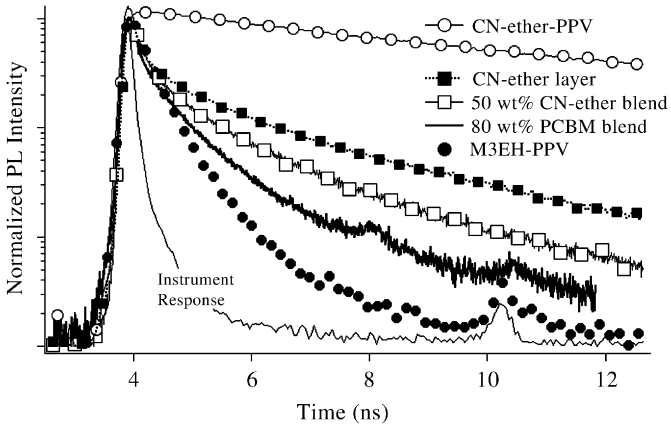

Fig. 5. Time-decay of photoluminescence intensity from TCSPC analysis.

4.4. PCBM

The use of PCBM, which efficiently separates excitons and transports electrons, has the expected effect of increasing device currents and efficiencies. FF increased as the wt% of PCBM in the blend was increased (Fig. 4) with a slope neatly mirroring the increase in current. This suggests that the same mechanism is responsible for the increase in each parameter; namely, the increased size of the PCBM domains which enhance electron-transport across the device. Devices with 20 wt% PCBM ($J_{sc} = 4.8\,mA/cm^2$, FF = 29%) are found to have lower currents and FF than those with 80 wt% of PCBM in the blend ($J_{sc} = 13\,mA/cm^2$, FF = 37%), under white light illumination. At 80 wt% PCBM, the ~40% FF of pristine M3EH-PPV devices on TiO_2//Au (in which transport is dominated by mobile holes) is regained. It is surprising that the peak FF is not higher due to the enhanced mobility of both electrons and holes upon the addition of PCBM. The FF has been found to exceed 60% in MDMO-PPV:PCBM cells [49]; a similar enhancement in FF in our devices would result in significant improvements in efficiency. It appears that charge transport is not as efficient in M3EH-PPV:PCBM cells due to poorer electron percolation or low hole mobility. Thus, our devices are not as well optimized as those reported by other groups, and provide a useful system for investigation of the factors that may limit device performance.

PCBM quenches the excited state more efficiently than CN-ether-PPV, but quenching remains incomplete as judged by the long-lived emission of M3EH-PPV (Fig. 5.) Low wt% blends are extremely well quenched, especially at short times; however, the lack of complete quenching suggests differences between our system and combinations of other PPV derivatives with PCBM, which tend to exhibit fast PL decays that are indistinguishable from the instrument response function. Contrary to the naïve assumption that more PCBM should result in increased charge transfer (shortening the lifetime), the rate of decay *increases* as the wt% of PCBM in the blend is *decreased*, counter to the enhanced device performance at high wt% of PCBM in the blend (Table 1). A less pronounced, but similar effect has been seen in TCSPC at low emission energies on MDMO-PPV:PCBM blends [50,51], attributable to long-lived emission from the PCBM phase. This attribution is supported by the fact that we see the decay component of PCBM grow in at 700 nm—the peak of PCBM emission.

Similarly, steady-state photoluminescence quenching is *less* efficient for 80 wt% compared to 20 and 50 wt% blends (see Ref. [52] for full details). These results are attributable to (a) better dispersion of the fullerene and (b) the absence of a long PCBM decay component for lower wt% PCBM in the blend. As in MDMO-PPV:PCBM blends, large domains of PCBM in 80 wt% blends presumably provide a continuous percolation pathway for the transportation of mobile electrons, resulting in high currents and FFs for high wt% PCBM blends. Thus, the ideal blend ratio for charge separation does not coincide with the ideal ratio for charge transport, due to blend morphology. In Fig. 6, an SEM cross-section of a 80 wt% M3EH-PPV:PCBM film reveals domain sizes on the order of tens of nanometers, similar to the 20 nm observed for MDMO-PPV [53]. Morphological changes in the blended film relative to the pristine polymer are also evidenced by a strong blueshift in the steady-state fluorescence. A new spectral peak of unknown origin is observed at 2.5 eV when the films are excited at low energy.

Photoluminescence decay from PCBM aggregates is detected in all heterojunctions. Decay from the PCBM phase is characterized by a time constant of 1.0–1.9 ns (see Table 1), which grows in at 700 nm emission—the peak of the (weak) PCBM emission. These aggregates reduce the surface area available for exciton dissociation, but increase the available charge percolation pathways, enhancing performance. Past a critical size, PCBM aggregates appear to be detrimental to device performance, based upon observations of blends of PCBM with

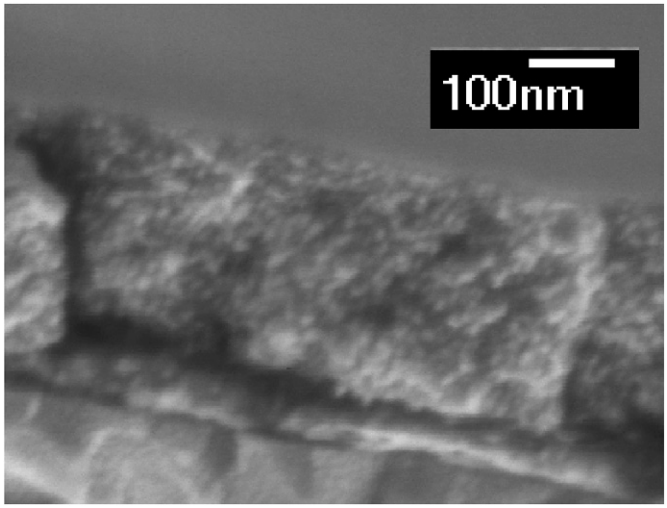

Fig. 6. SEM cross-section of M3EH-PPV:PCBM blend at 80 wt%.

poly-3-hexylthiophene (P3HT), which were characterized by large (>50 nm) aggregates and poor device performance. Given the high efficiencies found for M3EH-PPV:PCBM blends, further optimization of the underlying morphology of the polymer phase and the PCBM domain size could result in competitive device performances. A pathway for such improvement is suggested by an observed relationship between film morphology (both for pristine M3EH-PPV films and M3EH-PPV:PCBM blends) to changes in the spin-speed, thickness of the film, and solution concentration.

4.5. Comparisons

It was found that while the addition of PCBM enhanced device performance through an increase in the charge transport (indicated by a concomitant increase in FF) and exciton dissociation (indicated by TRPL quenching at short times), the same is *not* true for the addition of the electron-transporting polymer CN-ether-PPV. As seen in Fig. 4, the rise in device current in the polymer/polymer blend is a mirror image of the rise in FF, indicating that the charge transport suffers for the same reason as the device current is enhanced, namely the addition of CN-ether-PPV. The peak in FF does not mirror the peak in current for these devices. The destruction of efficient charge transport in polymer/polymer blends is a serious limitation, despite the enhanced exciton dissociation. As in PCBM devices, increasing amounts of CN-ether-PPV in the blend may create large domains. Morphology (i.e., domain size) is clearly critical for device performance, as also demonstrated by Quist et al. [54], who found that annealing of MDMO-PPV:CN-ether-PPV blends enhanced device performance primarily by creating larger CN-ether-PPV domains, thus reducing exciton recombination (exciton dissociation was not affected). Similar mechanisms are likely to affect our devices.

The quenching of the excited state in these two systems is less than expected. Table 1 shows that the quenching percentage ($Q = 1 - \tau_{\text{composite}}/\tau_{\text{neat film}}$) for the dominant decay time is around 75% for all heterojunctions with M3EH-PPV, despite dramatically enhanced device performance in PCBM blends. Quenching of the long-lived CN-ether-PPV excimer decay is more predictive of device performance, as is quenching of the steady-state photoluminescence. The strong CN-ether-PPV steady-state emission is quenched by ~90% in all heterojunctions (even in planar layers). Thus, it is easier to quench emissive species than non-emissive ones, presumably because rapid non-radiative recombination deactivates the excited state before charge transfer can occur.

The % yield represents the proportion of the steady-state photoluminescence attributable to a particular decay component; it is calculated by $\text{yield}\,(\%) = A_i\tau_i/\sum_j A_j\tau_j$, where A_i is the pre-exponential factor associated with the decay component τ_i. A comparison of % yield for these decay components across device architectures (Fig. 7) reveals the different exciton dynamics in the two systems. In PCBM blends (Fig. 7A), the population of the short-lived M3EH-PPV exciton ($\tau_1 = 0.20$ ns) decreases monotonically (and the population of the PCBM exciton, τ_3, increases) as additional PCBM is added to the blend, up to

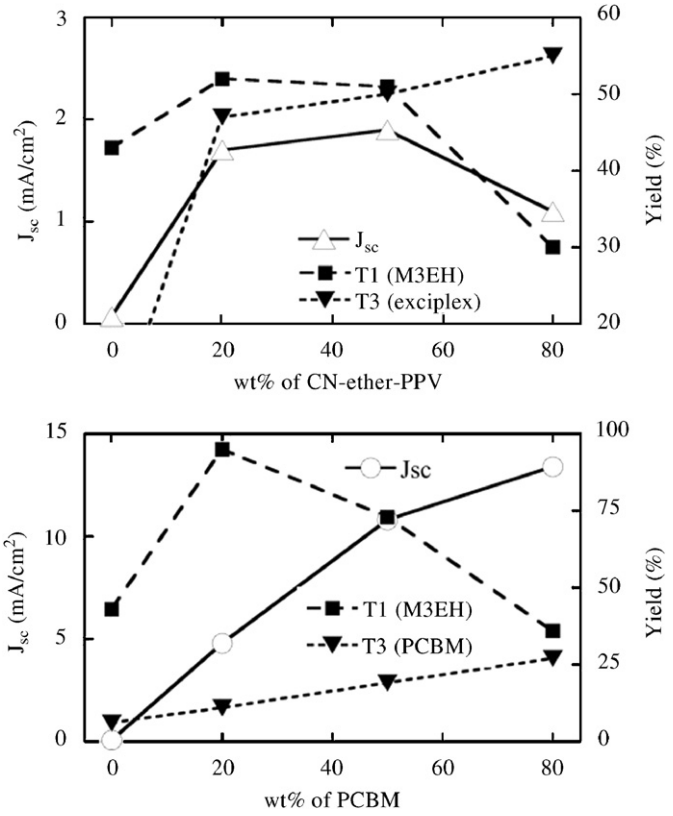

Fig. 7. Short-circuit current (open symbols) and % yields of decay components (closed symbols) in (A) M3EH-PPV:CN-ether-PPV blends, and (B) M3EH-PPV:PCBM blends. Emission is detected at the spectral peak for each component: 600 nm for T_1 (squares) and 700 nm for T_3 (triangles) in each case.

the peak performance at 80 wt% PCBM, as expected as the proportions of each element are varied. The same is not true for M3EH-PPV:CN-ether-PPV blends (Fig. 7B). The % yield for the M3EH-PPV τ_1 component does not decrease linearly as the wt% of CN-ether-PPV is increased, as would be expected due to a simple linear combination of the polymer components. Instead, the % yield of the M3EH-PPV τ_1 exciton is well correlated with the short-circuit current, suggesting that the same mechanism is responsible for the enhancement of each; namely, thermal re-excitation of M3EH-PPV excitons via exciplex decay. (Note that the exciplex τ_3 component increases linearly as CN-ether-PPV is added to the blend.) Thus, as in layered structures, exciton generation is extremely important for device performance in polymer/polymer blends.

The 0.45 ns decay component of M3EH-PPV was found to be particularly stubborn to quenching, and was only affected in low wt% PCBM blends. The existence of excitons that are impervious to quenching is detrimental to photovoltaic performance. The yield of this component (and thus the overall time-decay) co-varied with film thickness, presumably due to underlying film morphology differences caused by spin-speed, evaporation rate, and/or interaction with the substrate. Morphology can thus affect the time-decay of the excited state, outweighing the effects of charge-transfer.

In summary, our comparisons of several electron-transporting materials show:

- Photoluminescence lifetime is only loosely correlated with device performance due to morphological variations and intermediate states;
- Exciton dissociation is insufficient for optimization of device performance. Exciton generation (through the presence of exciplexes or layer thickness control) and charge transport pose more important limitations to performance;
- Morphology is critical in all aspects of device performance, from deactivation of the excited state to charge transport;
- Emissive interchain excitations may serve as useful sources of separable charge, whereas poorly emissive single-chain excitations are difficult to quench due to competing non-radiative rate constants.

5. Conclusions and implications

Our findings indicate that improved device performance does not necessarily relate directly to quenching of the excited state for the non-optimized devices reported here. While important, charge-transfer between materials is insufficient for optimization of device performance. Morphological effects of blending materials affects the decay parameters; exciton generation (seen in simulations of layered devices) and charge-transport (as evidenced in the relationship between FF and device performance in blended structures) must also be optimized. Morphology (chain conformation and domain size) is critical for peak exciton generation and subsequent charge transport, as well as reducing losses to recombination. This morphology is more easily controlled in layered device structures than in blended ones; however, the inherent obstacles to optimization of layered device structures require us to gain a better understanding and control of nanoscale morphology.

These current results also suggest that excitations in polymers cannot be treated with a simple decay model. For all polymer films, decay kinetics were multi-exponential, and these decay components were quenched incompletely and non-unilaterally. Thus, the decay kinetics are not well described by a simple model, in which a single excited state carrier relaxes to inter- and intra-chain species which may relax radiatively or non-radiatively. A complete understanding of the kinetics of excited states in polymer films requires that we broaden our description of excited state carriers to include the environment in which those carriers find themselves—such as a crystalline or non-crystalline film, in the middle or end of a chain, or trapped at a kink or defect in the polymer. These variables, which are intimately connected to underlying film and chain morphology, are all likely to affect the excited state kinetics and are difficult to control.

Future device performance may be enhanced through control of film thickness in layered devices, control of nanoscale morphology (such as domain size, or chain-stacking) leading to better charge transport, or through the use of materials with highly emissive interchain excitations and with exciplexes or other exciton scavengers. New imaging methods, such as conductive atomic force microscopy, will also further our understanding of the morphology of these films [55,56]. Further improvements of device performance will also be achievable through continued progress towards a deeper understanding of the morphologically mediated interplay between charge transport, generation, and exciton dissociation in polymer heterojunction films.

Acknowledgments

S.A.C. acknowledges support from the Beyond the Horizons program of DOE-NREL, contract ACQ-1-306-19-03, for this work. S.V.C. also acknowledges support from the Graduate Assistance in Areas of National Need (GAANN) scholarship.

The authors would like to thank Sean Shaheen and the scientists at the National Renewable Energy Laboratories (NREL) for both useful discussions and use of their equipment. S.V.C. would like to thank Marcus Jones, formerly of NREL, for providing the analytical tools and assistance necessary for fitting of TCSPC data. Numerical simulations were performed by Jan O. Haerter and Yuko Nakazawa.

References

[1] H. Hoppe, N.S. Sariciftci, J. Mater. Res. 19 (2004) 1924.
[2] S. Gunes, H. Neugebauer, N.S. Sariciftci, Chem. Rev. 107 (2007) 1324.

[3] K.M. Coakley, M.D. McGehee, Chem. Mater. 16 (2004) 4533.
[4] H. Spanggaard, F.C. Krebs, Sol. Energy Mater. Sol. Cells 83 (2004) 125.
[5] C.J. Brabec, N.S. Sariciftci, J.C. Hummelen, Adv. Funct. Mater. 11 (2001) 15.
[6] K. Kawano, R. Pacios, D. Poplavskyy, J. Nelson, D.D.C. Bradley, J.R. Durrant, Sol. Energy Mater. Sol. Cells 90 (2006) 3520.
[7] R. Pacios, A.J. Chatten, K. Kawano, J.R. Durran, D.D.C. Bradley, J. Nelson, Adv. Funct. Mater. 16 (2006) 2117.
[8] F.C. Krebs, J.E. Carle, N. Cruys-Bagger, M. Andersen, M.R. Lilliedal, M.A. Hammond, S. Hvidt, Sol. Energy Mater. Sol. Cells 86 (2005) 499.
[9] T. Jeranko, H. Tributsch, N.S. Sariciftci, J.C. Hummelen, Sol. Energy Mater. Sol. Cells 83 (2004) 247.
[10] G. Lungenschmied, G. Dennler, H. Neugebauer, S.N. Sariciftci, M. Glatthaar, T. Meyer, A. Meyer, Sol. Energy Mater. Sol. Cells 91 (2007) 379.
[11] F.C. Krebs, K. Norrman, Prog. Photovolt. Res. Appl. 15 (2007) 697.
[12] F.C. Krebs, H. Spanggaard, Chem. Mater. 17 (2005) 5235.
[13] G. Li, V. Shrotriya, J. Huang, Y. Yao, T. Moriarty, K. Emery, Y. Yang, Nature 4 (2005) 864.
[14] W. Ma, C. Yang, X. Gong, K. Lee, A.J. Heeger, Adv. Funct. Mater. 15 (2005) 1617.
[15] J.Y. Kim, K. Lee, N.E. Coates, D. Moses, T.-Q. Nguyen, M. Dante, A.J. Heeger, Science 317 (2007) 222.
[16] J. Nelson, Curr. Opin. Solid State Mater. Sci. 6 (2002) 87.
[17] C. Winder, N.S. Sariciftci, J. Mater. Chem. 14 (2004) 1077.
[18] C.J. Brabec, N.S. Sariciftci, Monatsh. Chem. 132 (2001) 421.
[19] S. Pfeiffer, H.-H. Hoerhold, Macromol. Chem. Phys. 200 (1999) 1870.
[20] A.J. Breeze, Z. Schlesinger, S.A. Carter, H. Tillmann, H.-H. Hoerhold, Sol. Energy Mater. Sol. Cells 83 (2004) 263.
[21] T.J. Savenije, J.M. Warman, A. Goossens, Chem. Phys. Lett. 287 (1998) 148.
[22] H. Tillmann, H.-H. Hoerhold, Synth. Met. 101 (1999) 138.
[23] S.C. Veenstra, W.J.H. Verhees, J.M. Kroon, M.M. Koetse, J. Sweelssen, J.J.A.M. Bastiaansen, H.F.M. Schoo, X. Yang, A. Alexeev, J. Loos, U.S. Schubert, M.M. Wienk, Chem. Mater. 16 (2003) 2503.
[24] J. Loos, X. Yang, M.M. Koetse, J. Sweelssen, H.F.M. Schoo, S.C. Veenstra, W. Grogger, G. Kothleitner, F. Hofer, J. Appl. Polym. Sci. 97 (2005) 1001.
[25] J.C. Hummelen, B.W. Knight, F. LePeq, F. Wudl, J. Yao, C.L. Wilkins, J. Org. Chem. 60 (1995) 532.
[26] G. Zerza, C.J. Brabec, G. Cerullo, S. De Silvestri, N.S. Sariciftci, Synth. Met. 119 (2001) 637.
[27] C.J. Brabec, G. Zerza, G. Cerulla, S. De Silvestri, S. Luzatti, J.C. Hummelen, N.S. Sariciftci, Chem. Phys. Lett. 340 (2001) 232.
[28] V.D. Mihailetchi, J. Wildeman, P.W.M. Blom, Phys. Rev. Lett. 94 (2005), (126602/1-4).
[29] A. Aharony, D. Stauffer, Introduction to Percolation Theory, second ed., Taylor & Francis, London, 1993.
[30] V.D. Mihailetchi, L.J.A. Koster, P.W.M. Blom, C. Melzer, B. de Boer, J.K.J. van Duren, R.A.J. Janssen, Adv. Funct. Mater. 15 (2005) 795.
[31] T.J. Savenije, J.E. Kroeze, M.M. Wienk, J.M. Kroon, J.M. Warman, Phys. Rev. B 69 (2004), (155205/1-11).
[32] R. Pacios, J. Nelson, D.D.C. Bradley, C.J. Brabec, Appl. Phys. Lett. 83 (2003) 4764.
[33] S.A. Choulis, J. Nelson, Y. Kim, D. Poplavskyy, T. Kreouzis, J.R. Durrant, D.D.C. Bradley, Appl. Phys. Lett. 83 (2003) 3812.
[34] C. Melzer, E. Koop, V.D. Mihailetchi, P.W.M. Blom, Adv. Funct. Mater. 14 (2004) 865.
[35] A.C. Arango, L.R. Johnson, V.N. Bliznyuk, Z. Schlesinger, S.A. Carter, H.-H. Hoerhold, Adv. Mater. 12 (2000) 1689.
[36] S.A. Carter, M. Angelopoulos, S. Karg, P.J. Brock, J.C. Scott, Appl. Phys. Lett. 70 (1997) 2067.
[37] A.C. Arias, M. Granstrom, K. Petritsch, R.H. Friend, Synth. Met. 102 (1999) 953.
[38] B.J. Schwartz, Annu. Rev. Phys. Chem. 54 (2003) 141.
[39] A.J. Breeze, Z. Schlesinger, P.J. Brock, S.A. Carter, Phys. Rev. B 64 (2001), (125205/1-9).
[40] D.V. O'Connor, D. Phillips, Time-correlated Single Photon Counting, Academic Press, London, 1984.
[41] S.R. Scully, M.D. McGehee, J. Appl. Phys. 100 (2006) 034907.
[42] S.V. Chasteen, J.O. Haerter, G. Rumbles, J.C. Scott, Y.K. Nakazawa, M. Jones, H.-H. Hoerhold, H. Tillmann, S.A. Carter, J. Appl. Phys. 99 (2006), (033709/1-10).
[43] I.D.W. Samuel, G. Rumbles, C.J. Collison, Phys. Rev. B 52 (1995) R11573.
[44] P.F. Miller, M.M. DeSouza, S.C. Moratti, A.B. Holmes, I.D.W. Samuel, G. Rumbles, Polym. Int. 55 (2006) 784.
[45] S.V. Chasteen, S.A. Carter, G. Rumbles, J. Chem. Phys. 124 (2006), (214704/1-6).
[46] J.O. Haerter, S.V. Chasteen, S.A. Carter, J.C. Scott, Appl. Phys. Lett. 86 (2005), (164101/1-3).
[47] A.C. Morteani, A.S. Dhoot, J.S. Kim, C. Silva, N.C. Greenham, C. Murphy, E. Moons, S. Cina, J.H. Burroughes, R.H. Friend, Adv. Mater. 15 (2003) 1708.
[48] T. Offermans, P.A. van Hal, S.C.J. Meskers, M.M. Koetse, R.A.J. Janssen, Phys. Rev. B 72 (2005), (045213/1-11).
[49] R.A.J. Janssen, J.C. Hummelen, N.S. Saricifti, MRS Bull. 30 (2005) 33.
[50] J.K.J. van Duren, X. Yang, J. Loos, C.W.T. Bulle-Liuwma, A.B. Sieval, J.C. Hummelen, R.A.J. Janssen, Adv. Funct. Mater. 14 (2004) 425.
[51] J.K.J. van Duren, X. Yang, J. Loos, C.W.T. Bulle-Lieuwma, A.B. Sieval, J.C. Hummelen, R.A.J. Janssen, Proc. SPIE 5215 (2004) 99.
[52] S.V. Chasteen, Ph.D. Thesis, University of California-Santa Cruz, 2005.
[53] T. Martens, J. D'Haen, T. Munters, Z. Beelen, L. Goris, J. Manca, M. D'Olieslaeger, D. Vanderzande, L. De Schepper, R. Andriessen, Synth. Met. 138 (2003) 243.
[54] P.A.C. Quist, T.J. Savenije, M.M. Koetse, S.C. Veenstra, J.M. Kroon, L.D.A. Siebbeles, Adv. Funct. Mater. 15 (2005) 469.
[55] X. Yang, J. Loos, Macromolecules 40 (2007) 1353.
[56] A. Alexeev, J. Loos, M.M. Koetse, Ultramicroscopy 106 (2006) 191.